Nanoscale

RSC Publishing

PAPER

View Article Online
View Journal | View Issue

Cite this: *Nanoscale*, 2013, **5**, 574

Band edge emission enhancement by quadrupole surface plasmon–exciton coupling using direct-contact Ag/ZnO nanospheres†

Yashu Zang,[a] Xu He,[a] Jing Li,*[a] Jun Yin,[ab] Kongyi Li,[a] Chuang Yue,[a] Zhiming Wu,[a] Suntao Wu[b] and Junyong Kang*[a]

Periodic Ag nanoball (NB) arrays on ZnO hollow nanosphere (HNS) supporting structures were fabricated in a large area by a laser irradiation method. The optimized laser power and spherical supporting structure of ZnO with a certain size and separation were employed to aggregate a sputtering-deposited Ag nano-film into an ordered, large-area, and two dimensional Ag NB array. A significant band edge (BE) emission enhancement of ZnO HNSs was achieved on this Ag NB/ZnO HNS hybrid structure and the mechanism was revealed by further experimental and theoretical analyses. With successfully fabricating the direct-contact structure of a Ag NB on the top of each ZnO HNS, the highly localized quadrupole mode surface plasmon resonance (SPR), realized on the metal NBs in the ultraviolet region, can effectively improve the BE emission of ZnO through strong coupling with the excitons of ZnO. Compared with the dipole mode SPR, the quadrupole mode SPR is insensitive to the metal nanoparticle's size and has a resonance frequency in the BE region of the wide band gap materials, hence, it can be potentially applied in related optoelectronic devices.

Received 25th September 2012
Accepted 15th November 2012

DOI: 10.1039/c2nr32906a

www.rsc.org/nanoscale

Introduction

In recent years, there has been increasing interest in the unique physical and chemical properties of metal nanostructures because of their fundamental and technological applications. The local surface plasmon resonance (SPR) effect, which is well understood as a coherent oscillation of the electrons in the local dielectric environment near the surface of metal nanoparticles (NPs), has been widely studied with potential applications in light emitting diodes (LEDs),[1] plasmonic solar cells,[2] photo-sensors,[3] biomedical sensors,[4,5] and so on. Several types of methods, such as electron or ion beam lithography[6,7] and chemical reduction,[8] have been developed to produce metal nanostructures. Both electron and ion beam lithography can create a large variety of geometries and patterns for nano-structures with high resolutions and tremendous flexibilities.[9,10] But low-throughput and high cost are always present in the fabrication processes. Unlike lithographic methods, chemical synthesis can prepare metal NPs in different shapes, but still shows its shortages with synthesized nanostructures with non-uniform sizes and random distributions.[11,12] Up to now, various metal nanostructures, such as nanostacks, hollow nanoshperes (HNSs), nanodisks, nanoflowers, *etc.*, have been successfully produced,[11–14] which present different properties and potential applications. However, it is still a challenge to achieve controllable preparation of the NPs in a large area with a uniform size and ordered distribution.

ZnO, as a versatile semiconductor material with a direct wide band gap (WBG) of 3.3 eV, has attracted attention because of its excellent performances in electronic and photonic devices.[15,16] To improve its light emission properties, employing metal NPs on ZnO based on the SPR effect can be considered as a promising method. On account of this idea, the energy match between surface plasmons (SPs) from metal NPs and excitons in semiconductor materials is the key factor to achieve enhanced luminescence.[17–19] Usually, the dipole plasmon resonance on metal NPs is the most easily realized mode among the SPR modes. However, the frequency of the dipole mode SPR is generally far away from the ultraviolet (UV) region, where the ZnO BE emission lies.[20] For metal NPs, *e.g.* Ag, only when the size of symmetric spherical NPs is smaller than 30 nm can the frequency of a dipole-mode SPR be modified near to the UV region.[21] On the other hand, the small nanoparticles have weak scattering intensity and a lower integrated scattering/absorption cross-section ratio according to the Mie theory,[22,23] which are not beneficial for the BE emission enhancement of a WBG semiconductor. It was also reported that a high order SPR can be feasibly obtained on highly symmetric spherical Ag NPs with

[a]*Department of Physic/Pen-Tung Sah Micro-Nano Institute of Science and Technology, Xiamen University, Xiamen, 361005, China. E-mail: lijing@xmu.edu.cn; jykang@xmu.edu.cn; Fax: +86-592-2187196; Tel: +86-592-2181340/2185962*

[b]*Wuhan National Laboratory for Optoelectronics, School of Optoelectronic Science and Engineering, Huazhong University of Science and Technology, Wuhan, 430074, China*

† Electronic supplementary information (ESI) available. See DOI: 10.1039/c2nr32906a

a larger size.[21] So the compromising between the realization of a certain SPR mode and the modification of Ag NP's size is a constructive proposal to practically apply metal NPs on a WBG semiconductor material, such as ZnO, to achieve an enhanced BE emission. The field strength of the quadrupole SPR mode attenuates more quickly with the distance by comparing with the dipole mode SPR. Thus, a local-contact structure is required with the aim to realize this high order SPR mode and employ it to achieve a BE emission enhancement in ZnO.

In this work, a technique based on a combination of nanosphere lithography (NSL) and pulse-laser-induced annealing was proposed to fabricate a large scale direct-contact Ag nanoball (NB)/ZnO HNS structure in an ordered and two-dimensional arrangement to significantly enhance the BE emission of ZnO. It is experimentally and theoretically evidenced that the fabricated Ag NB arrays with a certain size and separation can realize the quadrupole mode SPR in the UV region that is near the BE of ZnO. Given the strongly localized character of this high order SPR mode, the successful preparation of the direct contact Ag NB/ZnO HNS structure gives a full utilization of its intensive near field, which prominently enhances the ZnO BE emission *via* the effective energy coupling between the SPs and the excitons. This method provides a promising option for luminescence improvement in optoelectronic devices.

Experimental

The Ag NB/ZnO HNS composites were fabricated by the NSL self-assembly process and a subsequent pulsed laser irradiation. The schematic illustration of the process is depicted in Scheme 1.

The specific fabrication of ZnO HNS templates with different sizes adopted the same procedures as those in our previous work.[13] Briefly, the monolayer PS nanospheres (7 wt%) with a diameter of ~330 nm were firstly self-assembled on clean silicon substrates. The size and separation of the PS nanosphere template were manipulated by O_2 plasma etching with different durations. And then, a ZnO layer with a thickness of 20 nm was deposited on the PS templates at room temperature by radio-frequency (RF) magnetron sputtering. The ZnO hollow spherical structure was obtained by evaporating the PS spheres in the core using a thermal treatment at 500 °C for 30 minutes in ambient N_2. Meanwhile, this thermal treatment is helpful to improve the crystallinity of ZnO due to the Ostwald ripening effect in the annealing process.[24] Subsequently, a 20 nm Ag film was deposited on the ZnO HNS supporting structure using the RF magnetron sputtering. Finally, the samples were irradiated by a nanosecond pulsed excimer laser (Lambda-Physik COMPEX 205) in air to induce the rapid melting and phase transitions of the Ag thin film, resulting in crystalline Ag droplets. Due to the poor wetting between Ag droplets and the surface of the ZnO spherical hollow structure, Ag spherical NBs were formed on the top of the ZnO HNSs, as shown in Scheme 1f. For studying the transmission properties of the Ag NB/ZnO HNS composite structure, another sapphire substrate was applied to fabricate this structure. The morphologies and structure properties of the nanocomposites were investigated using a field-emission scanning electron microscopy (SEM) (Hitachi S-4800) and transmission electron microscopy (TEM) (JEM-2100) equipped with energy dispersive X-ray spectrum (EDX) analyzer. The crystal structures of the fabricated samples were characterized by a X-ray diffraction (XRD) (Panalytical X'pert PRO) with Cu Kα radiation (λ = 1.5406 Å) in a 2θ range of 20–65°. A UV-visible spectrophotometer (Varian Cary 300) was used to characterize the dispersive transmission coefficient T and a cathodoluminescence (CL) spectrometer (Model iHR320 Spectrometer System) was employed to study the emission properties of those samples. Temperature dependent time-resolved PL (TRPL) measurements were carried out to analyze the exciton recombination rate of the samples.

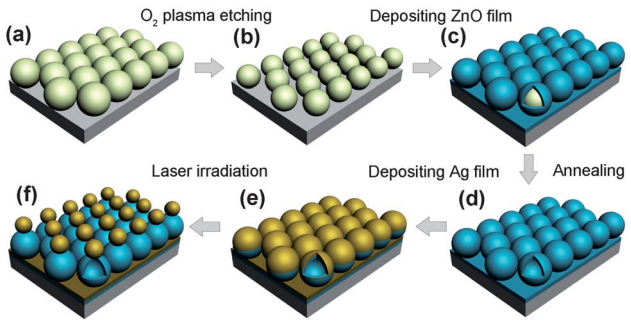

Scheme 1 A schematic illustration of the fabrication processes of a Ag NB/ZnO HNS hybrid structure: (a) self-assembled polystyrene (PS) nanosphere monolayer on Si substrate using the modified dip-coating method; (b) the PS nanosphere arrays etched by O_2 plasma for 0, 30, 60, and 90 seconds; (c) the as-deposited PS core/ZnO shell structure; (d) ZnO HNS arrays produced by annealing at 500 °C in N_2 ambient to evaporate the PS cores; (e) Ag film/ZnO HNS arrays; (f) Ag NB/ZnO HNS arrays obtained by laser irradiation.

Results and discussions

1 Optimization of the laser power on fabricating Ag NB/ZnO HNS composites

Fig. 1a–e show the SEM images of the Ag film/ZnO HNS samples irradiated under various laser power of 30, 60, 120, 150, and 190 mJ cm^{-2}. It can be observed that with the lower laser power irradiation of 30 mJ cm^{-2}, there is no obvious changes on the Ag

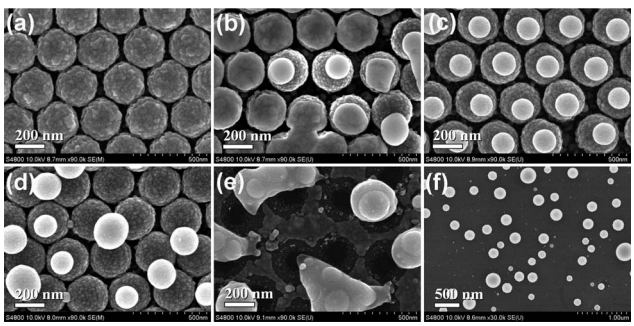

Fig. 1 SEM images of Ag film/ZnO HNS arrays irradiated by a laser beam with different powers of: (a) 30 mJ cm^{-2}, (b) 60 mJ cm^{-2}, (c) 120 mJ cm^{-2}, (d) 150 mJ cm^{-2}, and (e) 190 mJ cm^{-2}. And as a comparison, (f) the SEM image of Ag NPs aggregated from the Ag film coating on a Si substrate under the laser irradiation at the power of 190 mJ cm^{-2}.

film, as shown in Fig. 1a. While the laser power increases to 60 mJ cm^{-2}, the Ag film begins to melt and partially aggregates to Ag NBs or cap-shaped NPs, as displayed in Fig. 1b. Fig. 1c shows the ordered two-dimensional Ag NB arrays formed on the ZnO HNS structure as the laser power reaches 120 mJ cm^{-2}. Continuously increasing the laser power to 150 mJ cm^{-2}, the aggregated Ag NBs tend to gather with the neighboring ones to form larger NBs, as shown in Fig. 1d. Naturally, due to the melting of ZnO caused by the laser irradiation at the high power of 190 mJ cm^{-2}, Ag NB/ZnO HNSs completely collapse, as shown in Fig. 1e. As a result, the laser power of 120 mJ cm^{-2} is suitable to fabricate ordered Ag NB arrays on the ZnO HNS supporting structures.

As a comparison, a Ag film was deposited on a smooth Si substrate to demonstrate the Ag aggregation on different substrates. Clearly, the Ag film's aggregation on the Si substrate is much different from that on the ZnO HNS supporting structures as shown in Fig. 1f. It is verified that a higher laser power of 190 mJ cm^{-2} is required to induce the Ag film's aggregation to form Ag NPs on a flat Si substrate, which is in agreement with the previous literature.[25] Moreover, the size and distribution of Ag NPs on a Si substrate are not uniform, unlike those on a spherical-shaped supporting structure, such as on ZnO HNSs.

With regard to the formation of the Ag NB/ZnO HNS hybrid structure, it can be attributed to the photothermal effect in the Ag film under laser irradiation and poor wetting of the Ag droplets on the spherical ZnO HNS supporting structures. Since the silver's intrinsic interband absorption is in the UV region, the laser irradiation with a wavelength of 248 nm can be effectively absorbed by the Ag film.[26,27] When the absorbed energy is higher than the break-up threshold of these Ag films, the rising temperature will lead to the Ag aggregating into droplets due to the Rayleigh instability.[28] On the other hand, the poor wetting of the Ag on the ZnO spherical support structure will induce Ag droplets in the NB morphology standing on the top of each ZnO HNS with a big contact angle. Fig. 2a and b show the as-fabricated large area Ag NB/ZnO HNS arrays on the silicon substrate using the optimized laser power of 120 mJ cm^{-2}.

To control the size of Ag NBs, modification of the ZnO HNS template is proven to be an effective option. In our work, O_2 plasma etching with different durations was employed to adjust the PS nanospheres' size, thus the supporting ZnO HNSs with different separations and sizes were produced. Then as-prepared Ag film/ZnO HNS structures were irradiated with the optimized laser power of 120 mJ cm^{-2}. Fig. 3a–d show the Ag NB arrays on the different ZnO HNS supporting templates. The statistical size of ZnO HNS changes from 272 to 233 nm, while the Ag NB's size reduces from 159 to 132 nm as the etching duration increases from 0 to 90 s, as illustrated in Fig. 3e. There is an approximately linear relationship for the size distribution as a function of the etching duration, which can be used to quantitatively control the size of metal NPs in other applications.

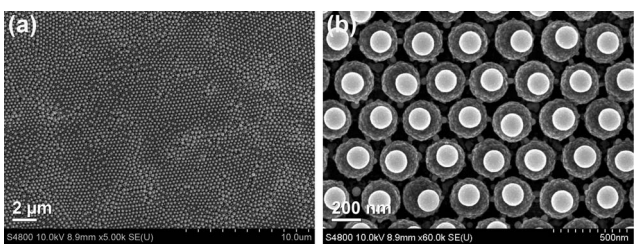

Fig. 2 SEM images of as-fabricated Ag NB/ZnO HNS arrays (a) in a large area and (b) in a higher magnification.

2 Crystal structures

To further investigate the structure properties of the as-fabricated Ag NB/ZnO HNS nanocomposite, XRD and TEM characterizations were carried out. The XRD patterns of the ZnO HNS, Ag film/ZnO HNS, and Ag NB/ZnO HNS structures are shown in Fig. 4, respectively. On all the samples, a dominant diffraction peak at 34.5° (2theta) was characterized as the wurtzite ZnO (002) plane diffraction, which indicates the preferential orientation along the wurtzite ⟨001⟩ direction in the ZnO HNS structure. It should be noted that the peak located at 38.1° (2 theta), corresponding to the Ag (111) plane, exhibits a stronger intensity in the Ag NB/ZnO HNS composite than that in the as-prepared Ag film/ZnO HNS sample. This can be attributed to the Ag NPs' recrystallization under the laser irradiation.

The more detailed information on morphologies and crystal structures of the Ag NB/ZnO HNS composite was obtained from the TEM images and selected area electron diffraction (SAED) patterns. Fig. 5a and b show the TEM images of the Ag film/ZnO HNS and the Ag NB/ZnO HNS composite structures after the laser irradiation treatment. It can be revealed that the morphology changes from the Ag film to Ag NBs except for a few small Ag nanograins left on the surface of the ZnO hollow supporting structure. This can also be evidenced from the energy dispersive spectrum (EDS) patterns, as shown in Fig. 5d and e, where the spectra were collected from the regions of the hollow structure of the Ag film/ZnO HNS and Ag NB/ZnO HNS

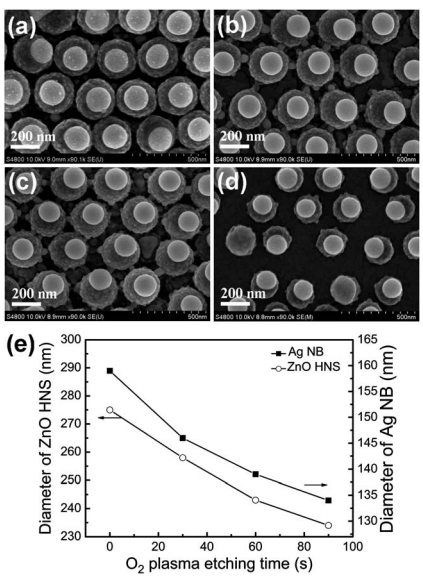

Fig. 3 SEM images of Ag NB/ZnO HNS arrays in various diameters controlled by employing the O_2 plasma etching on the PS template with different durations for (a) 0 s, (b) 30 s, (c) 60 s, and (d) 90 s, respectively. The size distributions of the Ag NBs and ZnO HNSs as a function of the etching time are illustrated in (e).

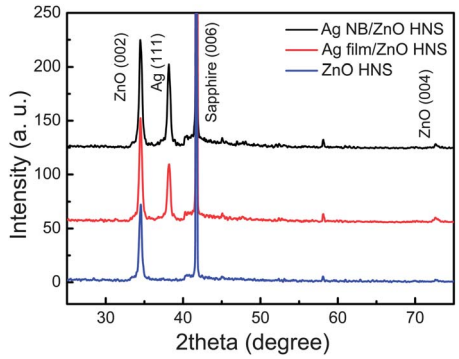

Fig. 4 XRD patterns of the Ag NB/ZnO HNS, Ag film/ZnO HNS, and bare ZnO HNS structures.

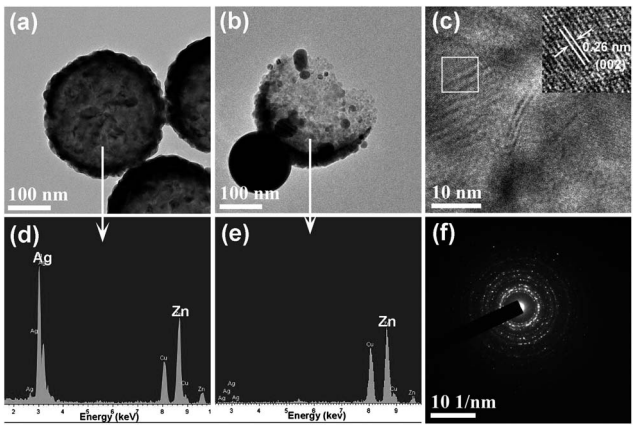

Fig. 5 TEM images of (a) Ag film/ZnO HNS, (b) Ag NB/ZnO HNS, and (c) the ZnO hollow area from (b) in high resolution (the inset image shows the lattice distance of the marked area); EDS patterns of (d) and (e) collected from the hollow structure areas in (a) and (b), respectively; (f) the SAED pattern of the hollow structure area in (b).

samples, respectively. Obviously, Ag content in the hollow region of the Ag NB/ZnO HNS sample is very low compared to that on the Ag film/ZnO HNS structure, since the Ag film evenly covers the surface of the ZnO HNS before the laser irradiation treatment. This indicates that the laser treatment can efficiently aggregate the Ag film into NBs. The high resolution TEM images in Fig. 5c taken from the ZnO hollow structure area of Ag NB/ZnO HNS sample present the interplanar spacing of ~0.26 nm corresponding to the lattice distance of the wurtzite ZnO (002) plane, which is also consistent with the XRD characterization results. The SAED pattern seen in Fig. 5f shows the polycrystalline characterization of the ZnO shell.

3 Enhanced BE emission of ZnO HNS

Fig. 6a shows the room temperature (RT)-CL spectra of the bare ZnO HNS and Ag NB/ZnO HNS composite. It can be seen that the ZnO HNS sample only exhibits a strong visible emission peak around 2.76 eV with the nearly resolved BE emission peak in the UV region. Generally, the BE emission of ZnO in the UV region is attributed to the exciton recombination, while the visible emission is related to the defects, such as interstitial zinc.[29,30] The low quality in this bare ZnO HNS sample is a normal character for ZnO prepared by a sputtering deposition. Compared with the bare ZnO HNS sample, a distinguishable BE emission at about 3.31 eV appears in the Ag NB/ZnO HNS sample, besides that the defect related emission has a similar intensity as that in ZnO HNS sample. By considering only the differences with or without the Ag NB's decoration on the two samples, it is suggested that the significant enhancement might be from the strong interaction between the SPs from Ag NBs and the excitons in ZnO. To confirm that the enhancement of CL is caused by the enhanced spontaneous recombination rate through the SP–exciton coupling, the temperature dependent TRPL at 3.31 eV (375 nm) was carried out and the results were analyzed.

The low temperature TRPL spectra of bare ZnO HNS and Ag NB/ZnO HNS structures are shown in Fig. 6b and the measured effective PL lifetimes are 60 and 28 ps, respectively. It is obvious that the recombination rate for excitons in ZnO was greatly improved after decorating with the Ag NBs, which is due to the SP–exciton coupling.[1,31,32] The temperature dependence of decay time for ZnO BE emission in those two samples is shown in the inset of Fig. 6b. It can be found that the recombination rate of excitons in ZnO HNS was enhanced as the temperature increased from 20 to 300 K, which is due to the delocalization of excitons and activation of the nonradiative recombination processes by the thermal energy. Compared with the bare ZnO HNS sample, the recombination rate of the Ag NB/ZnO is obviously enhanced in the entire temperature range and is stable as the temperature changes. Therefore, it can be concluded that the presence of Ag NBs enhances the spontaneous recombination rate, and thus the improvement of the ZnO BE emission can be attributed to the effective SP–exciton coupling process. To gain insight into the origin of this SP–exciton coupling enhanced BE emission, further transmission characterization and FDTD calculations were carried out.

The extinction spectra, including the absorption and scattering contributions, were deduced from the transmission spectra using the equation of $E = 1 - T$, where E and T are the extinction and transmission coefficient, respectively. The spectrum of the Ag NB/ZnO HNS sample is compared with those in the samples of the ZnO film, bare ZnO HNS structure, and Ag NP arrays, as shown in Fig. 7a. It can be noticed that there is a prominent peak at about 3.35 eV from both the ZnO film and ZnO HNS structure, which results from the ZnO BE absorption. Additionally, an absorption enhancement is observed in ZnO HNS arrays, which might be due to their nanostructure and spherical morphology. Furthermore, when Ag NBs were fabricated on this ZnO HNS array template, distinctive extinction properties were obtained and evidenced by the enhanced extinction at 3.35 eV and the presence of two additional extinction peaks around 2.38 and 3.93 eV. With considering the Ag NB's size of about 130 nm, the dipole mode SPR from the Ag NBs can be responsible for the broad peak around 2.38 eV.[33] For further studying the origins of the other two peaks, the extinction spectra of the Ag NP arrays are used to do a comparative analysis.

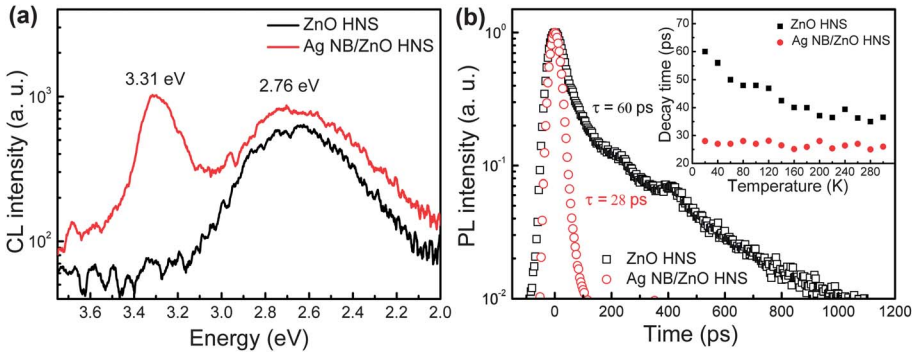

Fig. 6 (a) RT-CL spectra of ZnO HNS and Ag NB/ZnO HNS composite structures; (b) low temperature (20 K) TRPL spectra of ZnO HNS and Ag NB/ZnO HNS composite structures, the inset picture shows the decay time as the function of temperature.

For the sake of the consistence, the Ag NP arrays were produced by the laser irradiation on a 20 nm Ag film deposited on a sapphire substrate. Both peaks around 3.35 and 3.93 eV were observed in the spectrum of the Ag NP arrays. Thus, the enhanced extinction peak at about 3.35 eV in the Ag NB/ZnO HNS structure can be assigned to the overlap of the ZnO band edge absorption and the extinction of the Ag NPs, while the peak near 3.93 eV is from the interband absorption of silver.[26] Fig. 7b shows the extinction spectra of various Ag NB/ZnO HNS composite structures with different sizes adjusted by the O_2 plasma etching on PS nanosphere templates for 0, 30, 60, and 90 s, respectively. The above mentioned three pronounced extinction peaks can be seen in all the samples. With changing the Ag NB's size, the extinction peaks at about 3.35 and 3.93 eV have no obvious shifts. It's worth noting that with the size of Ag NBs reducing from 158 to 133 nm, the extinction peak induced by the dipole mode SPR undergoes a blue shift from 2.12 to 2.28 eV, which can be attributed to the size effect of metal NPs based on Mie's theory.[34]

To further understand the metal NPs' effect on the Ag NB/ZnO HNS system, the FDTD simulation was performed to calculate the absorption, scattering, and overall extinction cross sections of a single Ag NB model. Perfectly matched layer (PML) boundary conditions were used in the incident direction to

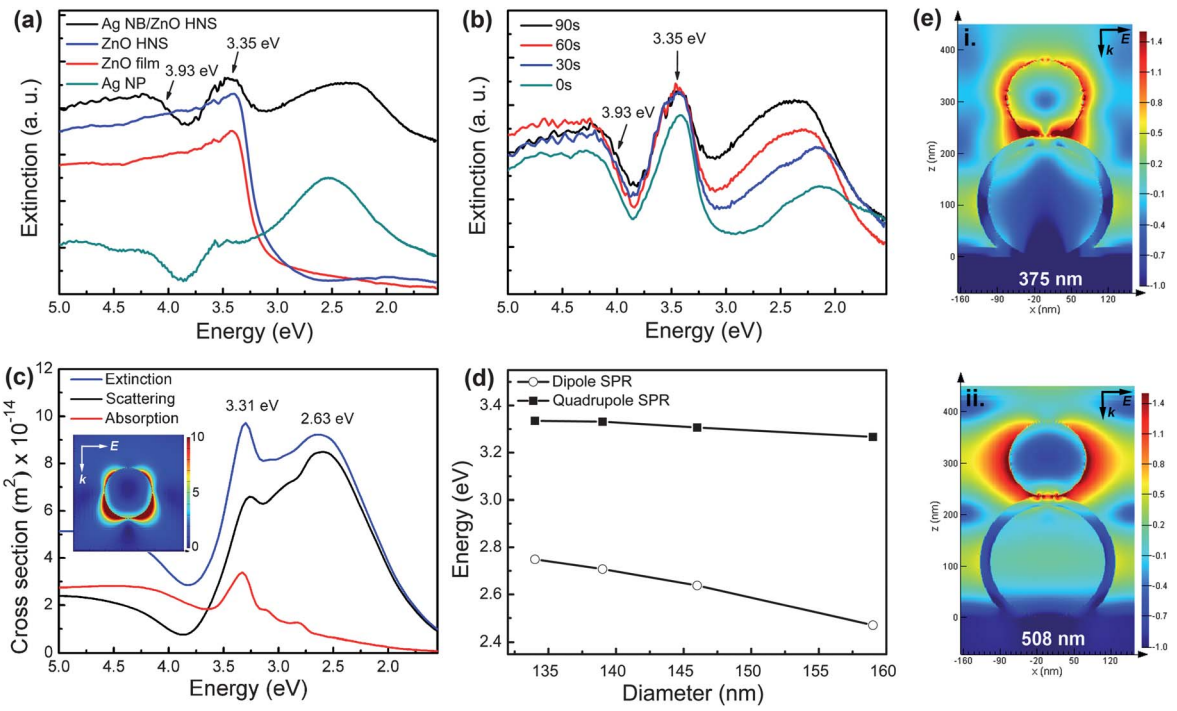

Fig. 7 UV-vis extinction spectra of: (a) Ag NB/ZnO HNS composite structure compared with those in the samples of the flat ZnO film, ZnO HNS structure, and Ag NP arrays; (b) Ag NB/ZnO HNS composite structures in different sizes adjusted by O_2 plasma etching on PS nanosphere templates for 0, 30, 60, and 90 s, respectively. And FDTD theoretical calculation of (c) absorption, scattering, and total extinction cross sections from a single Ag NB (inset shows the simulated near field distribution under 3.31 eV light illuminating for a single Ag NB and four-lobe field distribution pattern can be distinguished, (the intensity is in a linear scale)); (d) the relationship between the SPR frequency and the Ag NB's size. (e) Near-field distribution of quadrupole mode SPR at 375 nm (i) and dipole mode SPR at 508 nm (ii) from the Ag NB/ZnO HNS composite on the Si substrate (the intensity is in log scale).

prevent nonphysical scattering at the boundaries. Optical constants for Ag were taken from Palik[35] and fitted using the combined Drude and Lorentz model. Fig. 7c shows the simulated far-field optical properties from an isolated Ag NB in a diameter of 146 nm. It can be found that the profile of the obtained extinction spectrum is consistent with the experimental results except for a little shift of the corresponding peak position, as displayed in Fig. 7a. Those differences mainly come from neglecting the influence of the dielectric environment and the radiative coupling effect between the Ag NBs in the calculation model.[22,36] The extinction spectrum of a single Ag NB can be resolved with one broad peak located at about 2.63 eV and a sharper peak located around 3.31 eV. When the extinction spectrum is decomposed into its scattering and absorption contributions, the scattering dominates for the peak at about 2.63 eV, which is generally assigned to the dipole mode SPR. In order to verify the mechanism of the peak at about 3.31 eV, the near field distribution under 3.31 eV light illumination was calculated, as shown in the inset image of Fig. 7c, which shows the near-field distribution in the *xz* plane formed by the polarization and $\boldsymbol{k}$ vectors. The four-lobe field distribution proves the presence of the quadrupole mode SPR in the Ag NB.[37] This quadrupole mode SPR generally originates from the phase retardation from one side of the Ag NB to another and can be characterized as two parallel dipoles on opposite sides. Therefore, it is credible to attribute the extinction peak around 3.31 eV to the quadrupole mode resonance from the Ag NB, as well as the extinction enhancement in the BE region of ZnO contributed by the Ag NBs in the Ag NB/ZnO HNS structure, as shown in Fig. 7a. With considering the influence of the dielectric environment, the absorption, scattering, and overall extinction cross sections of the Ag NB/ZnO HNS composite have also been simulated, as shown in Fig. S1a of the ESI.† A similar spectrum profile as that in a single Ag NB system is obtained, except for the little shifts in relevant peak positions due to the influence of the ZnO dielectric environment and the unresolved peak in the UV region caused by the overlap of the ZnO BE absorption and the extinction of a Ag NB. The near-field distribution of the Ag NB/ZnO HNS hybrid structure under 3.31 eV (375 nm) and 2.44 eV (508 nm) light illumination were also simulated, as shown in Fig. 7e (i and ii), respectively. The notable four-lobe field distribution on the Ag NB/ZnO HNS composite indubitably evidences the quadrupole mode SPR in the UV region where the ZnO BE emission locates. Unlike the dipole mode SPR showing the field distribution on both sides of the Ag NB as usual, the quadrupole mode SPR induced near-field in the Ag NB/ZnO HNS system intensively re-distributes to the contact area between the Ag NB and ZnO HNS, as shown in Fig. 7e, which is responsible for the ZnO BE emission improvement by interacting with excitons in ZnO.

It can be noticed that the frequency of the dipole mode SPR in the simulated extinction spectra of the individual Ag NB and Ag NB/ZnO HNS also undergoes a red-shift with increasing size, as illustrated in Fig. 7d and Fig. S1b.† Combining the discussed results on the extinction spectra and FDTD calculation, the energy of quadrupole mode SPR from Ag NBs is at about 3.31 eV, which overlaps with the region of ZnO BE emission and has no significant shift. Thus it can be fully understood that the quadrupole SPs take a role in the strong interaction between the SPs of Ag NBs and the excitons in ZnO,[38] when the Ag NBs were fabricated on the ZnO HNS arrays. As mentioned above, the enhancement of the ZnO BE emission is generated by a possible mechanism of exciton–SP coupling. For SP–exciton coupling, there is a common view proposing that during the coupling process, the energy from excitons pumped by photos or electrons is transferred to SPs and then extracted as photon forms, in which a new recombination path is created.[19,38] In our work, the experimental and theoretical results demonstrate that both absorption and scattering of Ag NPs are considerable in the ZnO BE emission region, where the resonance happens between quadrupole SPs of Ag NBs and excitons in ZnO. For this reason, just based on this energy extraction mechanism it is not adequate to achieve a more than ten-times BE emission enhancement in Ag NB/ZnO HNS composite compared to bare ZnO film, as shown in the CL spectra of Fig. 6a, since both the absorption and scattering of Ag NBs would consume the light. Combined with the discussion of TRPL, the enhanced CL emission is mainly attributed to the increased exciton spontaneous recombination rate in the semiconductor material induced by the SP–exciton coupling process. When the energy of SP matches with that of the exciton, a strong coupling will occur between them. In this process, the recombination rate of the excitons can be significantly improved, resulting in a significant BE emission in the ZnO HNSs decorated by Ag NBs. It should be noticed that in our work the SPs are in quadrupole mode rather than in dipole mode as usually stated in previous works.

By resolving Laplace's equation, the near-field distribution of dipole and quadrupole SPs can be stated as the following:[37]

$$E_{\text{out}} = E_0\hat{x} + ikE_0\left(x\hat{x} + z\hat{z}\right) - \alpha E_0\left[\frac{\hat{x}}{r^3} - \frac{3x}{r^5}\left(x\hat{x} + y\hat{y} + z\hat{z}\right)\right]$$
$$-\beta E_0\left[\frac{x\hat{x} + z\hat{z}}{r^5} - \frac{5z}{r^7}\left(x^2\hat{x} + y^2\hat{y} + xz\hat{z}\right)\right]$$

where E_{out} is total local electric field intensity, E_0 is the electric field intensity of the incident electromagnetic, α and β are the sphere polarizability and $\hat{x}$, $\hat{y}$, and $\hat{z}$ are the usual unit vectors. The first and second parts in the right side of the equation are related to the *E*-field distribution of the dipole SPs, while the third and fourth parts describe the field distribution of the quadrupole SPs. It can be inferred from the equation that electrical field distribution of the quadrupole SPs attenuates more quickly with the increasing of *r* (the distance to the center of metal NPs) by comparing with the dipole SPs, which indicates that the field of quadrupole SPs is even more localized than the dipole SP's. In this work, the combination of NSL and laser irradiation method successfully proceeded to fabricate the direct contact structure of the Ag NB/ZnO HNS hybrid, in which the localized quadrupole mode SPR was realized and contributes to the significant BE emission in ZnO HNSs. Besides ZnO, in other WBG semiconductor materials, such as GaN or SiC, which have a similar band gap energy to ZnO, the BE emission enhancing is also an important issue needing to be resolved. So,

these Ag NB array structures can be potentially integrated into those materials to realize the manipulation of BE emissions using quadrupole SP–exciton coupling. Further applications in devices of LEDs or LDs can be reasonably proposed.

Conclusions

In this work, a novel technique based on a combination of NSL and pulsed-laser-induced annealing was proposed to fabricate Ag NB periodic arrays on the ZnO HNS supporting structure. By optimizing the laser power and choosing the proper PS nanosphere template, direct-contact Ag NB/ZnO HNS arrays with a controllable size and distribution were obtained. A significant ZnO BE emission enhancement in this hybrid structure was realized and the mechanism was demonstrated by experimental and theoretical works. In this unique direct-contact structure, quadrupole SPs with a resonance energy around 3.31 eV are locally excited. Due to the direct contact structure and the energy match between the quadrupole SPs and excitons in ZnO, the enhanced ZnO BE emission is accomplished by their strong coupling. Besides ZnO, this structure can also be easily integrated into other WBG semiconductor materials, such as GaN or SiC, to achieve luminescence enhancements and thus be potentially applied in optoelectronic devices.

Acknowledgements

The authors will present the great gratitude to Dr C. H. Chiu in SCLAB of NCTU in Taiwan for his kind help with the TRPL characterization. This work is financially supported by the MOST of China under the 973 programs (2009CB930704, 2011CB925600, and 2012CB619301), National Natural Science Foundation of China (61106118, 61227009, and 61106008), Natural Science Foundation of Fujian Province of China (2011J01362), and Fundamental Research Funds for the Central Universities (2011121026 and 2011121042).

Notes and references

1 K. Okamoto, I. Niki, A. Shvartser, Y. Narukawa, T. Mukai and A. Scherer, *Nat. Mater.*, 2004, **3**, 601.
2 V. E. Ferry, L. A. Sweatlock, D. Pacifici and H. A. Atwater, *Nano Lett.*, 2008, **8**, 4391.
3 J. L. Perchec, Y. Desieres and R. E. de Lamaestre, *Appl. Phys. Lett.*, 2009, **94**, 181104.
4 K. M. Mayer, F. Hao, S. Lee, P. Nordlander and J. H. Hafner, *Nanotechnology*, 2010, **21**, 255503.
5 S. Deng, H. M. Fan, X. Zhang, K. P. Loh, C. L. Cheng, C. H. Sow and Y. L. Foo, *Nanotechnology*, 2009, **20**, 175705.
6 G. R. Brewer, *Electron-beam Technology in Microelectronic Fabrication*, Academic Press, New York, 1980.
7 J. Melngailis, *J. Vac. Sci. Technol., B*, 1987, **5**, 469.
8 Y. L. Hou, H. Kondoh and T. Ohta, *Chem. Mater.*, 2005, **17**, 3994.
9 E. M. Hicks, S. L. Zou, G. C. Schatz, K. G. Spears and R. P. Van Duyne, *Nano Lett.*, 2005, **5**, 1065.
10 C. Y. Liu, A. Datta and Y. L. Wang, *Appl. Phys. Lett.*, 2001, **78**, 120.
11 M. Maillard, P. Huang and L. Brus, *Nano Lett.*, 2003, **3**, 1611.
12 N. R. Jana, L. Gearheart and C. J. Murphy, *J. Phys. Chem. B*, 2001, **105**, 4065.
13 J. Yin, Y. S. Zang, C. Yue, Z. M. Wu, S. T. Wu, J. Li and Z. H. Wu, *J. Mater. Chem.*, 2012, **22**, 7902.
14 Z. W. Cao, D. B. Xiao, L. T. Kang, Z. L. Wang, S. X. Zhang, Y. Ma, H. B. Fu and J. N. Yao, *Chem. Commun.*, 2008, (23), 2692.
15 Y. R. Ryu, T. S. Lee, J. A. Lubguban, H. W. White, Y. S. Park and C. J. Youn, *Appl. Phys. Lett.*, 2005, **87**, 153504.
16 Ü. Özgür, Y. I. Alivov, C. Liu, A. Teke and M. A. Reshchikov, *J. Appl. Phys.*, 2005, **98**, 041301.
17 P. H. Cheng, D. S. Li, Z. Z. Yuan, P. L. Chen and D. R. Yang, *Appl. Phys. Lett.*, 2008, **92**, 041119.
18 D. Y. Lei and H. C. Ong, *Appl. Phys. Lett.*, 2007, **91**, 211107.
19 Y. C. Lu, C. Y. Chen, D. M. Yeh, C. F. Huang, T. Y. Tang, J. J. Huang and C. C. Yang, *Appl. Phys. Lett.*, 2007, **90**, 193103.
20 D. D. Evanoff, Jr and G. Chumanov, *J. Phys. Chem. B*, 2004, **108**, 13948.
21 H. Tamaru, H. Kuwata and H. T. Miyazaki, *Appl. Phys. Lett.*, 2002, **80**, 10.
22 K. R. Catchpolea and S. Pillai, *J. Appl. Phys.*, 2006, **100**, 044504.
23 X. Chen, B. H. Jia, J. K. Saha, B. Y. Cai, N. Stokes, Q. Qiao, Y. Q. Wang, Z. R. Shi and M. Gu, *Nano Lett.*, 2012, **12**, 2187.
24 A. Krost, J. Christen, N. Oleynik, A. Dadgar, S. Deiter, J. Blasing, A. Krtschil, D. Forster, F. Bertram and A. Diez, *Appl. Phys. Lett.*, 2004, **85**, 1496.
25 S. J. Henley, J. D. Carey and S. R. P. Silva, *Appl. Phys. Lett.*, 2006, **88**, 081904.
26 C. M. Li, L. E. Urbach and H. L. Dai, *Phys. Rev. B: Condens. Matter*, 1993, **49**, 2104.
27 B. Balamurugana and T. Maruyama, *J. Appl. Phys.*, 2007, **102**, 034306.
28 J. Lian, L. M. Wang, X. C. Sun, Q. K. Yu and R. C. Ewing, *Nano Lett.*, 2006, **6**, 1047.
29 H. B. Zeng, Z. G. Li, W. P. Cai and P. S. Liu, *J. Appl. Phys.*, 2007, **102**, 104307.
30 N. S. Han, H. S. Shim, J. H. Seo, S. Y. Kim, S. M. Park and J. K. Song, *J. Appl. Phys.*, 2010, **107**, 084306.
31 I. Gontijo, M. Boroditsky, E. Yablonovitch, S. Keller, U. K. Mishra and S. P. DenBaars, *Phys. Rev. B: Condens. Matter*, 1999, **60**, 11564.
32 A. Neogi, C. Lee, H. O. Everitt, T. Kuroda, A. Tackeuchi and E. Yablonovitch, *Phys. Rev. B: Condens. Matter*, 2002, **66**, 153305.
33 C. P. Burrows and W. L. Barnes, *Opt. Express*, 2010, **18**, 3187.
34 G. Mie, *Ann. Phys.*, 1908, **330**, 377.
35 E. Palik, *Handbook of Optical Constants of Solids*, Academic, New York, 1985.
36 E. R. Encina and E. A. Coronado, *J. Phys. Chem. C*, 2010, **114**, 3918.
37 K. L. Kelly, E. Coronado, L. L. Zhao and G. C. Schatz, *J. Phys. Chem. B*, 2003, **107**, 668.
38 K. Okamoto, I. Niki and A. Scherer, *Appl. Phys. Lett.*, 2005, **87**, 071102.

